WAMS Based Damping Control of Inter-area Oscillations Employing Energy Storage System

Jing MA[1], Tong WANG[1, 2], James S. THORP[2], Zengping WANG[1], Qixun YANG[1], A. G. PHADKE[2]
[1] *State Key Laboratory for Alternate Electrical Power System with Renewable Energy Sources, North China Electric Power University, Beijing, 102206, China*
[2]*The Bradley Department of Electrical and Computer Engineering, Virginia Polytechnic Institute and State University, Blacksburg, VA, 24061, USA*
hdmajing@yahoo.com.cn

***Abstract*—This paper presents a systematic design procedure for a wide-area damping controller (WADC) employing Energy Storage Systems (ESSs). The WADC is aimed at enhancing the damping of multiple inter-area modes in a large scale power system. Firstly, geometric measures of controllability and obsevability are used to select the control locations for ESSs and most effective stabilizing signals, respectively. Then, the WADC coordinates these signals to achieve multiple-input-multiple-output (MIMO) controllers with the least Frobenius norm feedback gain matrix. The simulation results of frequency and time domains verify the effectiveness of the wide-area damping controller for various operating conditions. Furthermore, the robustness of the wide-area damping controller is also tested with respect to time delay and uncertainty of models.**

***Index Terms*—damping, energy storage, phasor measurement units, power system stability, robustness.**

I. INTRODUCTION

In recent times, with the significant reduction of the capital cost of the ESS, a new study of applications of energy storage system (ESS) in electric power systems is developed tremendously. An ESS unit installed in a power system provides an extra way of regulation and control, both the reactive and active power [1]. Therefore, the ESS increases the power system stability and security, which enables improved capacity utilization of the existing transmission lines and delays the requirement of installing new lines.

Apart from enhancing the transfer capacity of the transmission system, the ESS can also be used to increase the system damping for undesirable oscillations as a cost-effective damping controller [2]. Reference [3] presents the enhancing performance of local damping controller employing the ESS. However, it has been proved that under certain operating conditions an inter-area mode may be controllable from one area and be observable from another [4]-[6]. In these situations, information must be exchanged among areas. The technology of phasor measurement units (PMUs) has shown promising performance to enhance the damping of inter-area modes using the ESS [7]-[8]. However, due to inter-area uncoordinated control strategies used in many power systems, destabilizing interactions among ESS controls is possible. To improve overall system dynamic performance, the efficacy of a WAMS based damping feedback gain, functions are formulated to minimize interactions among ESS controls under transient controller employing ESSs is explored in this paper. The damping control technique considers the problem of assigning the eigenvalues associated with inter-area modes into a specified region in the left-half plane (LHP). By means of an optimization algorithm to select a desirable conditions, so that overall oscillation damping in the multi-machine system can be improved over a wide range of operating conditions.

Following this introduction, a description of a 16-machine-68-bus system model is given in Section 2. Section 3 provides techniques used in selection of control locations for ESSs and the most effective feedback control signals, and presents the mathematical basis wide-area damping control technique with the least Frobenius norm feedback gain matrix. Eigen-analysis and nonlinear simulation results have been carried out to assess the effectiveness of the proposed scheme under various fault scenarios and operating conditions in Section 4. The robustness with respect to model uncertainty and time delays are also tested in this section. The conclusion is given in Section 5.

II. STUDY SYSTEM

A. System Modeling

A benchmark model of 16-machine-68-bus, five-area study system is shown in Figure 1 for considering the design of damping controller. This is a reduced order equivalent of the interconnected New England test system (NETS) and New York power system (NYPS). There are five geographical regions out of which NETS and NYPS are represented by a group of generators. The loads are assumed to be of constant impedance type for the base case.

G1-G8 in group 5 have slow excitation (IEEE type DC1A), while a fast-acting static exciter is located at machine G9. A speed-input power system stabilizer is also installed in this particular machine, as described in [9]. A sixth-order model for each generator is used for simulation in this paper. For the convenience of the analysis, the sixth-order model is then transformed to a second-order model by using selective model analysis (SMA) [10]. The detailed description of the study system including generators,

Project Supported by the National Basic Research Program of China (2012CB215200), by National Natural Science Foundation of China (50907021，50837002), by the Chinese University Scientific Fund Project (11MG01,09QX64), by the Project Sponsored by the Scientific Research Foundation for the Returned Overseas Chinese Scholars (State Education Ministry([2011]1139), and by Hebei Natural Science Foundation (E2012502034).

Digital Object Identifier 10.4316/AECE.2012.02006

exciters, network and load parameters can be found in [11]. There are four inter-area modes obtained from the eigenvalue analysis as shown in Table I.

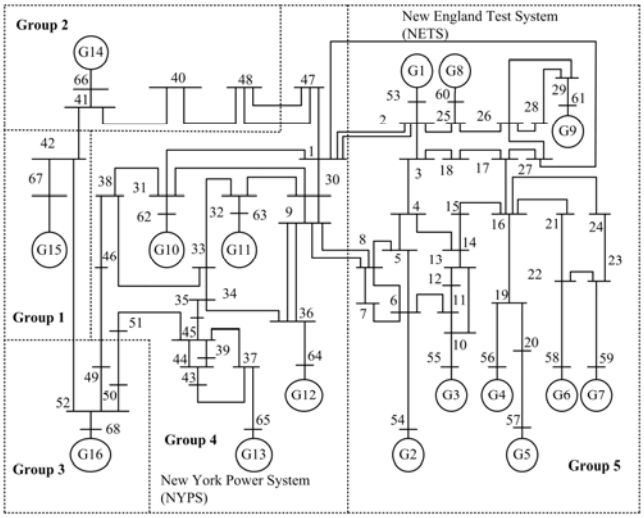

Figure 1. 16-machine, five-area study system.

TABLE I. DOMINANT INTER-AREA MODES AND PARTICIPATED GENERATORS OF THE STUDEY SYSTEM

Mode	Frequency(Hz)	Damp ratio	Dominant participated generator
1	0.4803	0.0516	G12 G13 G16
2	0.5034	0.0358	G14 G16
3	0.7112	0.0647	G1~G9 G13
4	0.7908	0.0337	G14 G15 G16

The most probable contingencies occurring in power systems are outages of key tie lines, changes in the power flow through the tie line and variations in load characteristics. In this paper, a few credible contingencies are investigated in Table II. The first case is defined as the base case with constant impedance (CI). Cases 2-3 consider constant current (CC), and constant power (CP), respectively. Cases 4-6 reflect the operating scenarios with one of the tie lines between buses1-2, 8-9, and 1-27 switched off, respectively. Cases 7-9 represent the changed operating conditions. Cases 10 and 11 correspond to -500 MW and 500 MW through tie line 1-2, respectively. Cases described in Table II will be used to test the robustness of controllers.

TABLE II. CASE BANK

Case No.	Case	Type of load
1(base)	No outage Flow from buses 2 to 1 =90MW	CI
2	No outage	CC
3	No outage	CP
4	One of double circuit line 1-2	CI
5	One of double circuit line 8-9	CI
6	1-27	CI
7	10% decrease in Inertial of equivalent at generator 14	CI
8	110% load	CI
9	90% load	CI
10	Flow from buses 2 to 1 =500MW	CI
11	Flow from buses 1 to 2=500MW	CI

B. ESS modeling

A general model is derived for all types of ESS which is referred to as the injection model is valid for load flow and angle stability analysis [12] as shown in Figure 2. Speed deviation measurements are used as the global feedback input signals in this paper.

Due to fast but not negligible time response, small time delays are introduced in small signal model of an ESS unit. As shown in Figure 3, the model is formed as a transfer function with lag element, having a time constant T_{ess} and a gain **K** between the frequency deviation $\Delta\omega$ and the incremental ESS power to injection ΔP_{ess}

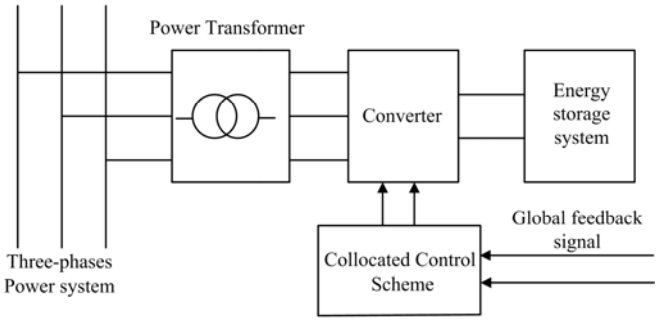

Figure 2. ESS structure and interconnection diagrams.

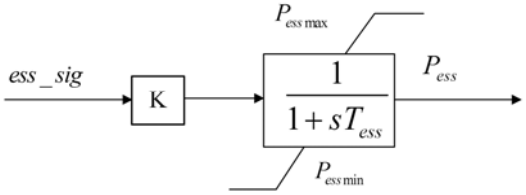

Figure 3. Small signal model of an ESS unit.

III. WIDE-AREA DAMPING CONTROLLER DEIGN

A. Selection of location and effective signals for controllers

From an economic viewpoint, it is worthwhile to use fewer stabilizing signals to improve the damping effects of many inter-area modes achieve satisfactory damping. The geometric measures of controllability (GMC) and observability (GMO) [13]-[15] are carried out to identify the locations and most effective input stabilizing signals for ESSs. The GMC and GMO corresponding to the mode *k* are

$$gm_{ci}(k) = \cos(\alpha(\psi_k, b_i)) = \frac{\left|b_i^T \psi_k\right|}{\|\psi_k\|\|b_i\|} \quad (1)$$

$$gm_{oj}(k) = \cos(\beta(\phi_k, c_j)) = \frac{\left|c_j \phi_k\right|}{\|\phi_k\|\|c_j\|} \quad (2)$$

where b_i is the *i*th input vector of **B** and c_j is the *j*th output vector of **C**. ψ and ϕ are left and right eigenvectors of state matrix **A**, respectively. ψ_k and ϕ_k are left and right eigenvector with respect to the *k*th mode respectively. $\alpha(\psi_k, b_i)$ is the geometrical angle between ψ_k and b_i. $\beta(\phi_k, c_j)$ is the geometrical angle between ϕ_k and c_j. $\|\psi_k\|$ and $\|b_i\|$ are the Euclidean norm of ψ_k and b_i, respectively. $\|\phi_k\|$ and $\|c_j\|$ are the Euclidean norm of ϕ_k and c_j, respectively $\left|b_i^T \psi_k\right|$ and $\left|c_j \phi_k\right|$ are the modulus of $b_i^T \psi_k$ and $c_j \phi_k$, respectively.

The most suitable locations with respect to critical inter-area modes are the buses with the highest GMC as shown in

Table III. And effective input stabilizing signals with respect to critical inter-area modes are the rotor speeds with highest GMO as shown in Table IV. It is revealed that buses 65, 67, and 68 (shown in boldface) are the best locations and ω_{13}, ω_{14}, and ω_{15} are the best stabilizing signals. Here ω_{13}, ω_{14}, and ω_{15} indicate the generator rotor speeds of generators 13, 14, and 15 versus the reference generator 16, respectively.

TABLE III. NORMALIZED GEOMETRIC MEASURES OF CONTROLLABILITY OF ALL POSSIBLE BUSES

Mode 1		**Mode 2**		**Mode 3**		**Mode 4**	
Bus No.	GMC	Bus No.	GMC	Bus No.	GMC	Bus No.	GMC
65	**1.0000**	**68**	**1.0000**	**67**	**1.0000**	**65**	**1.0000**
42	0.9296	52	0.9312	42	0.9757	37	0.7368
67	0.9039	41	0.7878	66	0.6282	43	0.5770
41	0.8321	66	0.7862	41	0.6027	44	0.5708
66	0.8216	50	0.3833	68	0.4100	39	0.4855
37	0.8182	42	0.2120	52	0.3176	36	0.3585
68	0.6718	67	0.2082	40	0.1368	16	0.3186
43	0.6542	40	0.1811.	50	0.1184	24	0.3167
52	0.6490	51	0.1313	48	0.0695	15	0.3144
44	0.6479	48	0.0943	65	0.0580	17	0.3123

TABLE IV. NORMALIZED GEOMETRIC MEASURES OF OBSERVABILITY OF ALL GENERATOR ROTORS

Mode 1		**Mode 2**		**Mode 3**		**Mode 4**	
Gen No.	GMO	Gen No.	GMO	Gen No.	GMO	Gen No.	GMO
13	**1.0000**	**14**	**1.0000**	**13**	**1.0000**	**15**	**1.0000**
15	0.9875	5	0.7088	6	0.9475	13	0.3055
6	0.9863	6	0.6948	7	0.9421	5	0.2858
7	0.9811	7	0.6941	5	0.9176	6	0.2810
4	0.9684	9	0.6921	4	0.9025	7	0.2805
9	0.9622	4	0.6910	9	0.7990	4	0.2795

B. Wide-area damping controller synthesis

The behavior of a dynamic power system can be written in the following from using vector-matrix notation.

$$\begin{bmatrix} \Delta\dot{\boldsymbol{\delta}} \\ \Delta\dot{\boldsymbol{\omega}} \\ \dot{\boldsymbol{\mu}} \end{bmatrix} = \begin{bmatrix} \mathbf{0} & \omega_0\mathbf{I} & \mathbf{0} \\ \mathbf{A_{21}} & \mathbf{A_{22}} & \mathbf{A_{23}} \\ \mathbf{A_{31}} & \mathbf{A_{32}} & \mathbf{A_{33}} \end{bmatrix} \begin{bmatrix} \Delta\boldsymbol{\delta} \\ \Delta\boldsymbol{\omega} \\ \boldsymbol{\mu} \end{bmatrix} + \begin{bmatrix} \mathbf{0} \\ \mathbf{0} \\ \mathbf{B_3} \end{bmatrix} \mathbf{u} \tag{3}$$

where $\Delta\boldsymbol{\delta}$ and $\Delta\boldsymbol{\omega}$ are vectors of the deviations of angles and rotor speeds of n generators, respectively. $\boldsymbol{\mu}$ is the $m\times 1$ states vector associated with the ESS controllers chosen. $\mathbf{u}\in\mathbf{R}^m$ is the control inputs vector. $\mathbf{B}_3\in\mathbf{R}^{n\times m}$ is the input matrix. Expressing $\Delta\dot{\boldsymbol{\omega}}$ in terms of the state variables yields

$$\Delta\dot{\boldsymbol{\omega}} - \mathbf{A_{22}}\Delta\boldsymbol{\omega} - \mathbf{A_{21}}\Delta\boldsymbol{\delta} = \mathbf{A_{23}}\boldsymbol{\mu} \tag{4}$$

Substituting $\Delta\dot{\boldsymbol{\delta}} = \omega_0\Delta\boldsymbol{\omega}$ to Eq. (4) which results in Eq. (5)

$$\Delta\ddot{\boldsymbol{\delta}} - \mathbf{A_{22}}\Delta\dot{\boldsymbol{\delta}} - \omega_0\mathbf{A_{21}}\Delta\boldsymbol{\delta} = \omega_0\mathbf{A_{23}}\boldsymbol{\mu} \tag{5}$$

Additionally, the basic idea in the inter area oscillation problem of power system can be formulated into modal coordinates as Eq. (6).

$$\Delta\ddot{\boldsymbol{\delta}} + \mathbf{D}\Delta\dot{\boldsymbol{\delta}} + \mathbf{K}\Delta\boldsymbol{\delta} = \mathbf{B}\mathbf{u} \tag{6}$$

where $\Delta\boldsymbol{\delta}\in\mathbf{R}^n$ is the vector of deviations of angles. $\mathbf{B}\in\mathbf{R}^{n\times m}$ is the control influence matrix. $\mathbf{D}$ and $\mathbf{K}$ are damping matrix and stiffness matrix, respectively.

Compared Eq. (6) with Eq. (5), $\mathbf{B}$, $\mathbf{D}$ and $\mathbf{K}$ can be obtained. $\mathbf{D} = -\mathbf{A_{22}}$, $\mathbf{K} = -\omega_0\mathbf{A_{21}}$, and $\mathbf{B} = \omega_0\mathbf{A_{23}}$.

To relocate the open-loop eigenvalues associated with the critical modes to stable region so that the critical modes have desired damping, a feedback gain $\mathbf{Q}$ in Eq. (7) is then selected to damp critical inter-area modes.

$$\boldsymbol{\mu} = -\mathbf{Q}\mathbf{B}^{\mathbf{T}}\Delta\dot{\boldsymbol{\delta}} \tag{7}$$

Then, substituting (7) to (6) which yields

$$\Delta\ddot{\boldsymbol{\delta}} + (\mathbf{D} + \mathbf{B}\mathbf{Q}\mathbf{B}^{\mathbf{T}})\Delta\dot{\boldsymbol{\delta}} + \mathbf{K}\Delta\boldsymbol{\delta} = \mathbf{0} \tag{8}$$

The term $\mathbf{BQB^T}$ is nonnegative definite matrix as a multidimensional resistive network, which can be used to design multiple-input-multiple-output (MIMO) controllers. Additionally, since $\mathbf{BQB^T}$ is nonnegative definite, it is not harmful for the damping added by the feedback even though the system model varies.

Any closed loop eigenvalue λ of (8) is calculated as

$$\left|\lambda^2\mathbf{I} + (\mathbf{D} + \mathbf{B}\mathbf{Q}\mathbf{B}^{\mathbf{T}})\lambda + \mathbf{K}\right| = 0 \tag{9}$$

The objective of the oscillation damping is to relocate the open-loop eigenvalues associated with the critical modes to some region so that the critical modes have desired damping. To be specific, the feedback gain $\mathbf{Q}$ is calculated by mapping the λ plane in which the eigenvalues of Eq. (10) reside to the γ plane. If γ plane is mapped from λ plane, the eigenvalues of Eq. (10) are calculated as

$$\gamma = \frac{r - c + \lambda}{r + c - \lambda}, \lambda = \frac{r(\gamma - 1)}{\gamma + 1} + c \tag{10}$$

where r and c are radius and center of a circle, respectively.

By this mapping, the eigenvalues in the left half of the γ plane are placed to the λ plane in stable region.

Substitute Eq. (10) into Eq. (9), which results in

$$\left|\mathbf{M}\gamma^2 + \mathbf{N}\gamma + \mathbf{P}\right| = 0 \tag{11}$$

where $\mathbf{M} = (r+c)^2\mathbf{I} + (r+c)(\mathbf{D} + \mathbf{B}\mathbf{Q}\mathbf{B}^{\mathbf{T}}) + \mathbf{K}$,

$\mathbf{N} = -(r^2 - c^2)\mathbf{I} + c(\mathbf{D} + \mathbf{B}\mathbf{Q}\mathbf{B}^{\mathbf{T}}) + \mathbf{K}$,

$\mathbf{P} = (r-c)^2\mathbf{I} - (r-c)(\mathbf{D} + \mathbf{B}\mathbf{Q}\mathbf{B}^{\mathbf{T}}) + \mathbf{K}$.

It can be seen that the solutions of Eq. (9) lie in stable region if and only if the solutions of Eq. (11) lie in left half region. If $\mathbf{M}\ge 0$, $\mathbf{N}\ge 0$ and $\mathbf{P}\ge 0$, then the solutions of Eq. (11) lie in left half region. Since $r\ge 0$, $c\ge 0$, and $\mathbf{M}\ge 0$ for any nonnegative definite matrix $\mathbf{Q}$, it can be concluded that the eigenvalues of system Eq. (9) lie in stable region if and only if the feedback gain $\mathbf{Q}$ satisfies $\mathbf{N}\ge 0$ and $\mathbf{P}\ge 0$. Furthermore, excessively feedback gain $\mathbf{Q}$ is inhibited, because it could lead to a poor large disturbance response of the system and controller output saturation. To avoid large feedback gain $\mathbf{Q}$, the real parts of the closed loop eigenvalues are restricted to be close to an optimal negative number, which means the least energy consumption in implementing the feedback control. Thus, the problem of determining feedback gain $\mathbf{Q}$ can be considered as the least Frobenius norm problem. This problem can be formulated as the following constrained optimization problem. The feasible region of the constrained optimization problem is a convex subset in $\Re^{m\times m}$ and the objective function is a convex function, therefore the solution to this problem is unique and globally minimum.

The actual values of optimized gain matrix $\mathbf{Q}$ is

$$\begin{bmatrix} 11.5852 & -2.1358 & 4.5172 \\ -2.1358 & 10.7495 & -0.7665 \\ 4.5172 & -0.7665 & 21.4333 \end{bmatrix}.$$

$\boldsymbol{\delta}$ and $\boldsymbol{\omega}$ are internal machine variables. If we measure bus angles $\boldsymbol{\theta}$ and frequencies $\dot{\boldsymbol{\theta}}$ in the system (as many as the number of internal angles and frequencies are required) and then Eq. (12) and Eq. (13) can be obtained.

$$\boldsymbol{\delta} = f(\boldsymbol{\theta}, \mathbf{x}_L, \mathbf{U}_b, \mathbf{I}) \quad (12)$$

$$\boldsymbol{\omega} = g(\dot{\boldsymbol{\theta}}, \mathbf{x}_L, \mathbf{U}_b, \mathbf{I}) \quad (13)$$

where $\mathbf{x}_L$ is a vector of impedances between generator outlets and generator buses, $\mathbf{U}_b$ is vector of buses voltage phasor measured by PMUs, $\mathbf{I}$ is vector of the circuit measured by PMUs.

The applied widely control technique is the single objective synthesis, in which all control requirements are weighted and formulated. For complex cases, such as unstable plants with multiple gain crossover frequencies, it may not be easy to decide on a desired loop shape. To overcome these limitations of a single objective synthesis technique, the multi-objective synthesis technique incorporating various design specifications easily, is naturally considered. In the design process, the wide-area measurements system (WAMS) based ESSs devices is applied to design a wide-area damping control system. The control synthesis is centralized and the stabilizing signals are firstly sent to a wide-area damping controller (WADC) through communication links. Then, modulation signals are determined by the WADC and are sent to three ESSs, as shown in Figure 4.

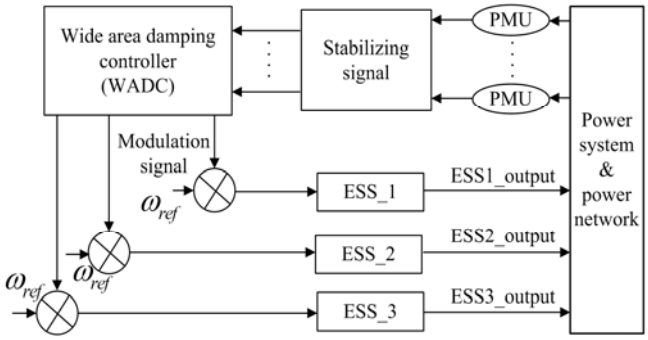

Figure 4. Wide-area damping controller synthesis configuration

IV. Testing Results and Analysis

A. Frequency domain results and analysis

The frequency domain analysis of the study system is carried out for various scenarios shown in Table V. It shows that three ESSs improve the damping of all four critical inter-area modes to a satisfactory level. Figure 5 shows the root loci for the gain ranging from 0 to 100% of the chosen gain. The c_i on Figure 5 show which control is responsible for that branch of the root locus. c_1 moves the fourth eigenvalue, c_2 moves the second eigenvalue and c_3 moves the first and third eigenvalues. It can be concluded that lack of any ESS controller will not damp all four modes to guarantee the overall system dynamic stability.

The performance of wide-area damping controller (WADC) is also evaluated with the outages of different tie-lines; various load characteristic and other operating conditions. The damping action shown in cases 1-3 robustness with respect to the outage of each of the tie-lines demonstrate the robustness of the damping action in case of various load models, such as CI, CP, and CC. Cases 4-6 is between buses 1-2, buses 8-9, and buses 1-27 which connects NETS and NYPS. Cases 7-9 represent the robustness of the damping action in case of other operating conditions. It is clear from the results that the WADC provide damping for different operating conditions.

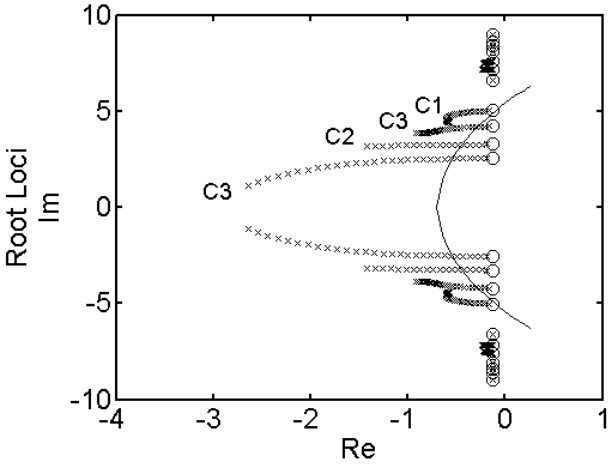

Figure 5. The root loci for the base case.

Bode plots of frequency responses of the study system for each ESS device in the case of open and closed loops are shown in Figure 6. It can be seen that the peaks in the gain of frequency responses of the open-loop system are noticeable around inter-area mode frequency. But the peaks in the gain of frequency responses of the closed-loop system are negligible around inter-area mode frequency. Furthermore, the phase angles of frequency responses of the open-loop system are changing dramatically. But the phase angles of frequency responses of the closed-loop system are changing smoothly. Both negligible peaks in the gain and negligible changes in the phase angle of frequency responses demonstrate high damping in the case of closed loop.

B. Time domain results and analysis

Two nonlinear simulations both have been carried out for 25s to further demonstrate performance and robustness of the controllers without any prior knowledge of the post-disturbance dynamics.

TABLE V. DAMPING RATIOS AND FREQUENCIES OF INTER-AREA MODES WITH WADC

Case No.	Mode 1		Mode 2		Mode 3		Mode 4	
	f(Hz)	Damp ratio	f(Hz)	Damp ratio	f(Hz)	Damp ratio	f(Hz)	Damp ratio
1	0.1589	0.9419	0.4996	0.2969	0.5893	0.2084	0.7975	0.1224
2	0.1860	0.9208	0.4929	0.3331	0.6049	0.1777	0.7963	0.1230
3	0.1778	0.9642	0.5068	0.3068	0.5871	0.1994	0.7962	0.1232
4	0.1604	0.9113	0.4953	0.1781	0.5527	0.3257	0.7979	0.1241

5	0.1591	0.9718	0.5093	0.1680	0.5400	0.3387	0.7979	0.1236
6	0.1590	0.9219	0.5153	0.2651	0.5588	0.2408	0.7976	0.1232
7	0.2131	0.9470	0.5041	0.2882	0.5879	0.2207	0.7685	0.1419
8	0.1534	0.9332	0.5181	0.3577	0.6127	0.1417	0.7983	0.1223
9	0.0987	0.9295	0.4216	0.3527	0.5529	0.2122	0.7942	0.1247
10	0.1813	0.9139	0.4596	0.1479	0.5677	0.3520	0.7982	0.1218
11	0.0823	0.9522	0.4739	0.3960	0.6597	0.1134	0.7946	0.1266

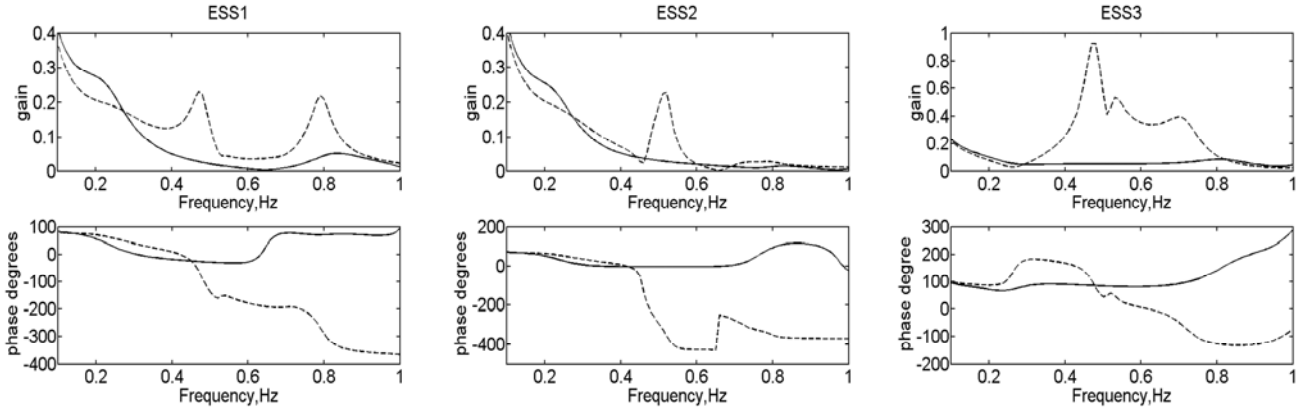

Figure 6. Frequency responses of the study system for ESSs in case of open and closed loops (full plant) (--) open loop; (-) closed loop.

In the first case, a three-phase short circuit fault was applied to tie line between buses 1-2. The fault was then cleared after 80 ms (approximately 5 cycles) by taking out the faulted line. The case is certainly not the most severe contingence but it is effective for exciting inter-area oscillations and evaluating the performance of the WADC. The dynamic response of the system following this contingency is shown in Figures 7-8.

The relative angular separations between machines G1-G16, G13-G16, G14-G16, and G15-G16 are shown in Figure 7. It can be seen that the lightly damped oscillations are settled in 12–15 s in the presence of the applied control scheme. A 10–15-s settling is adopted by many utilities in their system design and operation guidelines. Power flow in the tie-line between buses 8-9 and also the output responses of the three ESSs following the large disturbance are shown in Figure 8. It can be seen that the power flow between buses 8 and 9 also settles within the acceptable time frame. The outputs of the three ESSs are well within their prescribed limits. The simulation results illustrate that the WADC is able to achieve the desired performance without any prior knowledge about the post-disturbance operating conditions.

In the second case, a three-phase fault was simulated at tie line between buses 8-9 for 80 ms without changing the system topology, followed by the opening of one of the tie lines connecting buses 1 and 2 (see Figure 1). The dynamic response of the system following this contingency is shown in Figures 9-10.

The displays in Figure 9 show the relative angular separations between machines G1-G16, G13-G16, G14-G16, and G15-G16. It can be seen that the inter-area oscillations are damped out in 12-15 s. Figure 10 shows the power flow in the tie-line between buses 1-27 and the output responses of the three ESSs following the large disturbance. Power flow between buses 1 and 27 also settles within the acceptable time frame. The outputs of the three ESSs are well within their prescribed limits. The simulation results illustrate that, even though the knowledge of the post-disturbance operating condition is absent, the performance of the WADC is found to be highly acceptable. The absolute value of the largest output of an ESS is the energy rating when active power is expressed in MW. It was found that energy rating of 70 MJ, 40 MJ and 100 MJ could provide adequate damping performance for ESS #1， ESS #2 and ESS #3 respectively.

In addition to system nonlinearity, the controllers are subjected to saturation of the ESSs. To better illustrate the damping affected by the limited power output of the ESSs, an output limit of 20 MW and 50 MW are also set for each ESS, separately. The relative angular separations between machines G1-G16, G13-G16, G14-G16, and G15-G16 are shown in Figure 11-12. Power flow in the tie-line between buses 8-9 and output responses of three ESSs following the large disturbance of the first case are shown in Figures 12-13. It can be seen that the power flow on the tie line settles within 15 s though the settling time is a little longer than the case with 50 MW output limit. On the other hand, the power outputs of three ESSs are in the saturation values for a little longer time, but are still within their prescribed limits.

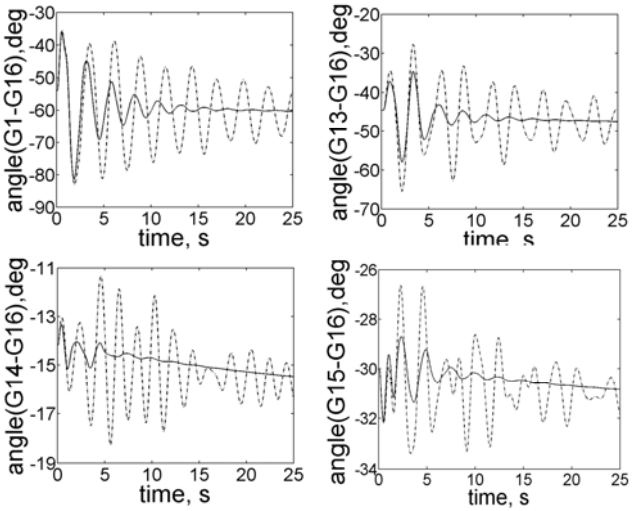

Figure 7. Dynamic responses of the system following a three-phase fault on line 1-2. (-) with controller; (--) without controller.

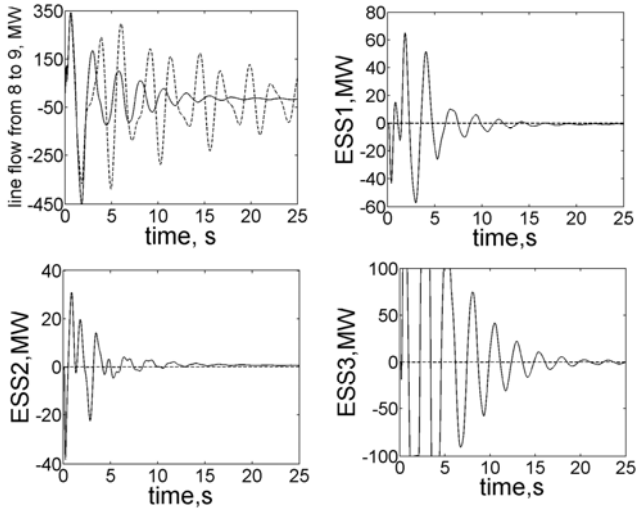

Figure 8. Dynamic responses of controllers following a three-phase fault on line 1-2. (-) with controller; (--) without controller.

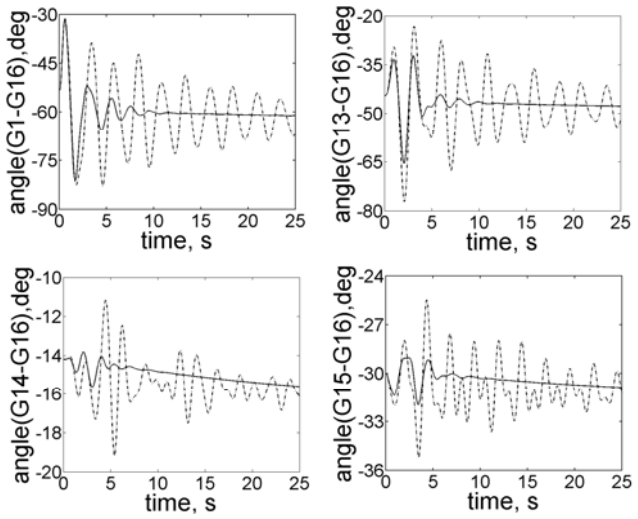

Figure 9. Dynamic response of the system following line 1-2 three-phase fault in case of opening of one of the tie lines connecting buses 8 and 9. (-) with controller; (--) without controller.

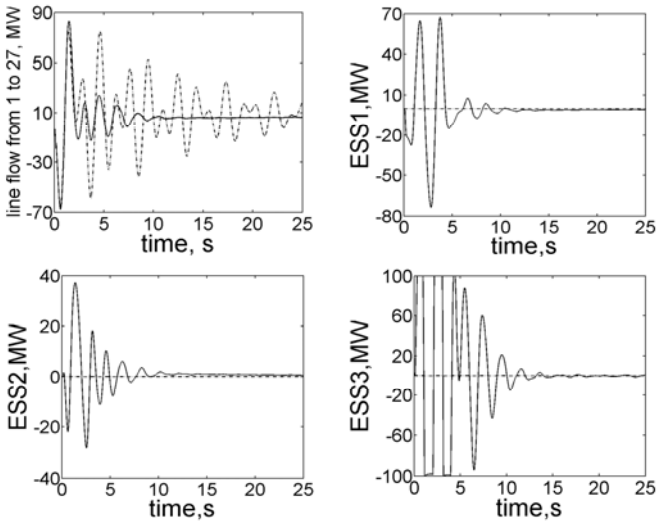

Figure 10. Dynamic responses of the controllers following a three-phase fault on line 1-2 in case of opening of one of the tie lines connecting buses 8 and 9. (-) with controller; (--) without controller.

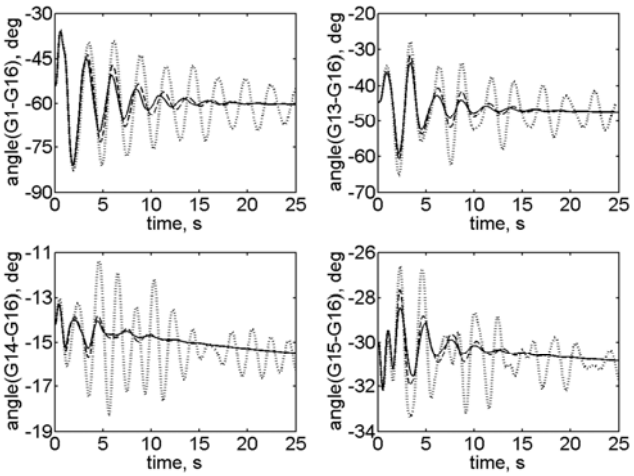

Figure 11. Dynamic responses of the system following a three-phase fault on line 1-2. (—) with limited power output of 50 MW ; (---)with limited power output of 20 MW. (...) without controller.

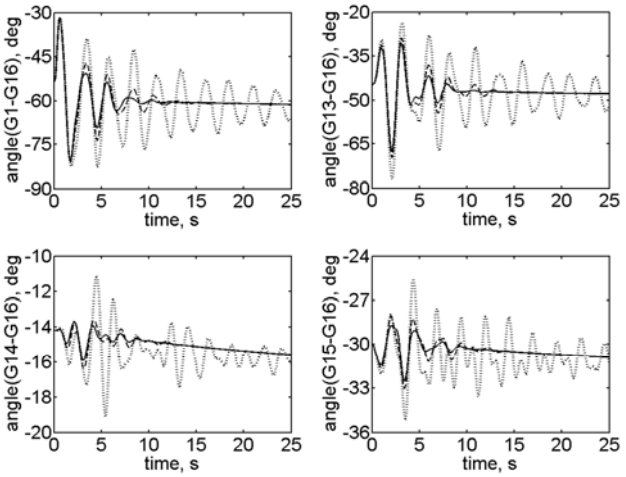

Figure 12. Dynamic response of the system following line 1-2 three-phase fault in case of opening of one of the tie lines connecting buses 8 and 9. (—) with limited power output of 50 MW ; (---)with limited power output of 20 MW. (...) without controller.

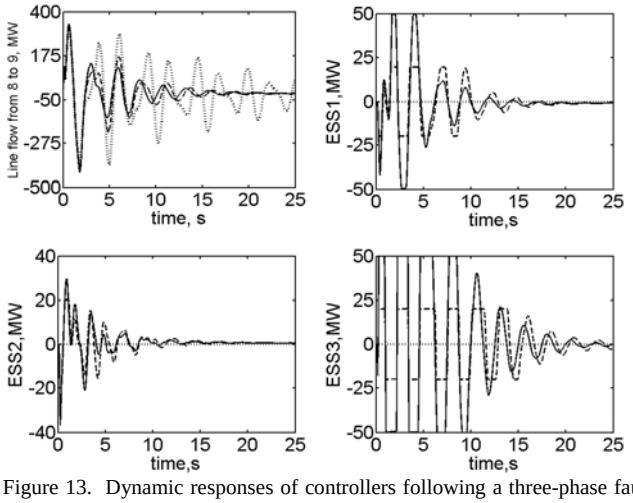

Figure 13. Dynamic responses of controllers following a three-phase fault on line 1-2. (—) with limited power output of 50 MW ; (---)with limited power output of 20 MW. (...) without controller.

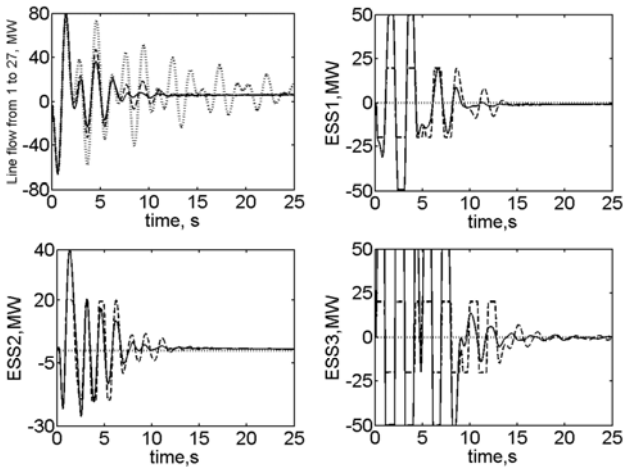

Figure 14. Dynamic responses of the controllers following a three-phase fault on line 1-2 in case of opening of one of the tie lines connecting buses 8 and 9. (—) with limited power output of 50 MW ; (---)with limited power output of 20 MW. (...) without controller.

C. Robustness of WADC

In addition to changing operating conditions to test for robustness it can be more systematic by considering structured uncertainty in the parameters of the model. Assume that the system structure can be exactly matched in the control. That is, if the model is

$$\begin{bmatrix}\dot{\mathbf{x}}_1\\ \dot{\mathbf{x}}_2\end{bmatrix}=\begin{bmatrix}\mathbf{0} & \mathbf{I}\\ -\mathbf{K} & -\mathbf{D}\end{bmatrix}\begin{bmatrix}\mathbf{x}_1\\ \mathbf{x}_2\end{bmatrix}+\begin{bmatrix}\mathbf{0}\\ \mathbf{B}\end{bmatrix}\mathbf{u},\quad \mathbf{u}=-\mathbf{Q}\mathbf{B}_c{}^{\mathrm{T}}\mathbf{x}_2 \tag{14}$$

The matrix $\mathbf{B}_c$ is probably not exactly the matrix $\mathbf{B}$. If we let $\mathbf{B}_c=\mathbf{B}+\Delta\mathbf{B}$ then one characterization of $\Delta\mathbf{B}$ is that every element in $\mathbf{B}_c$ could be in some interval around the true value.

There is literature in power system [16]-[17], control system [18]-[20], and structural [21]-[23] applications of interval valued uncertainty. In simulation we could multiply each entry in $\mathbf{B}$ by an independent uniform random variable q_{ij} in [0.8 1.2], for example, representing a +/- 20% error. The eigenvalues of (15) will generally be in clouds in the complex plane clustered around the desired positions.

$$\begin{bmatrix}\mathbf{0} & \mathbf{I}\\ -\mathbf{K} & -\mathbf{D}-\mathbf{B}\mathbf{Q}\mathbf{B}^{\mathrm{T}}-\mathbf{B}\mathbf{Q}\Delta\mathbf{B}^{\mathrm{T}}\end{bmatrix} \tag{15}$$

Figure 15 shows the clouds formed by having all 45 entries in $\mathbf{A}_{23}$ multiplied by an independent uniform random variable in the interval [0.8 1.2]. Figure 15 is the clouds around the ends of the loci in Figure 5 for 10,000 independent trials. It can be seen that the clouds are still in the stable region even if the system model changes.

On the other hand, time delays associated with the transmission of remote signals may also degrade system robustness. Therefore, the robustness of WADC with respect to different time delays is needed to be tested. Time delays are approximated as a first-order model [24]. And nonlinear simulations with 200 ms and 400 ms time delays for the second case are carried out to demonstrate the robustness with respect to time delays as shown in Figure 16. The simulation results show that the power flow in the tie line 1-27 can be settled within the acceptable time frame in the cases of different time delays though the damping time becomes a little longer due to time delays.

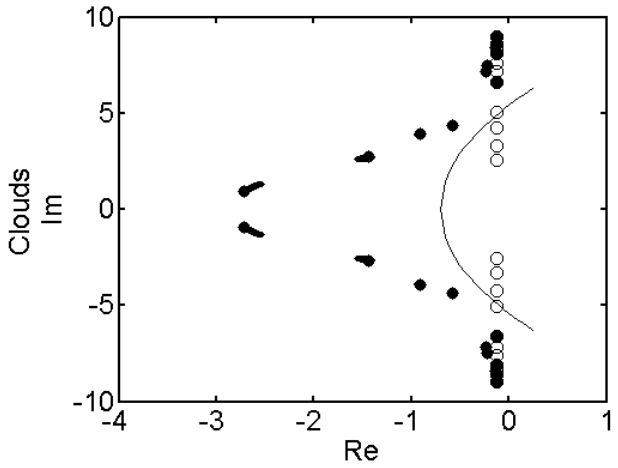

Figure 15. The clouds for the base case

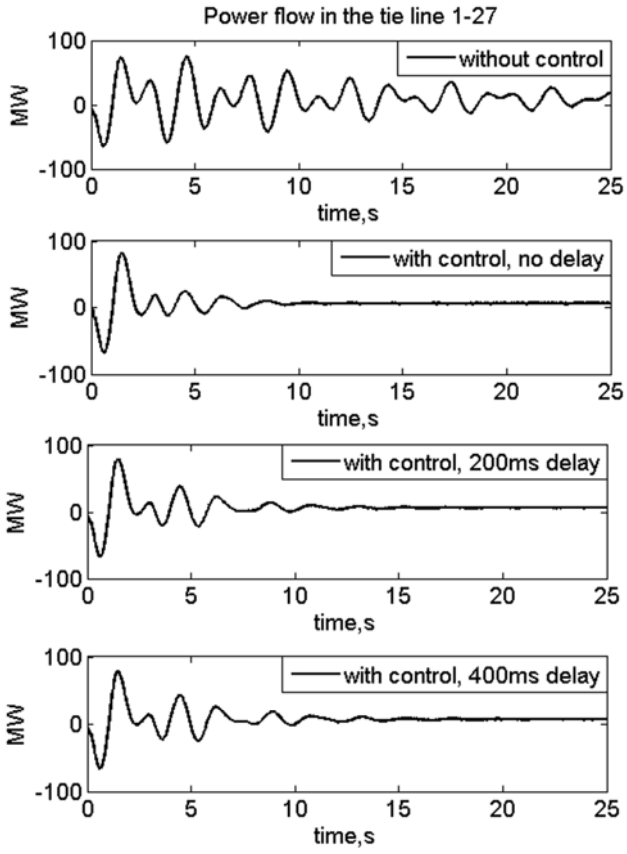

Figure 16. Dynamic responses of system under different time delays.

V. CONLUSION

The application of wide-area damping of inter-area oscillations by ESSs devices has been demonstrated in this paper. The most suitable locations and effective input stabilizing signals with respect to critical inter-area modes are selected by geometric measures of controllability (GMC) and observability (GMO), respectively. Also, a desirable feedback gain is selected by means of an optimization algorithm to minimize interactions among ESS controls. Furthermore, a wide-area damping controller is also designed to coordinate these stabilizing signals and achieve the multi-objective control. Finally, the effectiveness of the control scheme has been verified in the time and frequency domains under a wide range of conditions. Furthermore,

from the simulation results, it can be concluded that the action of designed wide-area damping controller shows robustness with respect to time delay and uncertainty of models.

ACKNOWLEDGMENT

Many faculties and students contribute greatly to this research. The authors would like to thank Dr. Yilu Liu.

REFERENCES

[1] Hasan Ali, Bin Wu, Roger A. Dougal, "An overview of SMES applications in power and energy systems," *IEEE Trans. on Sustainable Ener.*, vol. 1, no. 1, pp. 38-47, Apr. 2010.

[2] Du W., Wang H. F., Dunn R., "Power system oscillation stability and control by FACTS and ESS-a survey," *International Conference on Sustainable Power Generation and Supply*, pp. 1-13, Nanjing, China, Apr.6-7, 2009.

[3] Bharat Bhargava, Gary Dishaw, "Application of an energy source power system stabilizer on the 10 MW battery energy storage system at Chino substation power systems," *IEEE Trans. on Power Syst.*, vol.13, no.1, pp.145-151, Feb. 1998.

[4] Kamwa, I., Robert Grondin, Yves Hébert, "Wide-area measurement based stabilizing control of large power systems-a decentralized/hierarchical approach," *IEEE Trans. on Power Syst.*, vol. 16, no.1, pp. 136-153, Feb. 2001.

[5] A. Elices, L. Rouco, H. Bourles, and T. Margotin, "Physical interpretation of state feedback controllers to damp power system oscillations," *IEEE Trans. on Power Syst.*, vol, 19, no. 1, pp. 436-443, Jan. 2004.

[6] Francis Okou, Louis-A. Dessaint, Ouassima Akhrif, "Power systems stability enhancement using a wide-area signals based hierarchical controller," *IEEE Trans. on Power Syst*., vol. 20, no.3, pp. 1465-1477, Aug. 2005.

[7] Bikash C. Pal, Alun H. Coonick, Donald C. Macdonnld Robust, "Damping controller design in power systems with superconducting magnetic energy storage devices," *IEEE Trans. on Power Syst.*, vol. 15, no. 1, pp. 320-325, Feb. 2000.

[8] M. H. Ali, T. Murata, and J. Tamura, "A fuzzy logic-controlled superconducting magnetic energy storage (SMES) for transient stability augmentation," *IEEE Trans. Control Syst. Technol.*, vol. 15, no. 1, pp. 144–150, Jan. 2007.

[9] P. Kundur, *Power System Stability and Control*. New York: McGraw-Hill, 1994.

[10] I. J. Perez-Arriage, G. C. Verghese, and F. C. Schweppe, "Selective modal analysis with applications to electric power systems, Part I: Heuristic introduction," *IEEE Trans. on Power Syst*., vol. PAS-101, no. 9, pp. 3117-3125, Sep. 1982.

[11] G. Rogers, *Power System Oscillations.* MA: Kluwer, 2000.

[12] Bikash C. Pal, Alun A. Coonick, Imad M. Jaimoukha, Haitham El-Zobaidi, "A linear matrix inequality approach to robust damping control design in power systems with superconducting magnetic energy storage device," *IEEE Trans. on Power Syst.* vol. 15, no.1, pp. 356-362, Feb. 2005.

[13] Yang Zhang, Anjan Bose, "Design of wide-area damping controllers for interarea oscillations," *IEEE Trans. on Power Syst.*, vol. 23, no. 3, pp. 1136-1143, Aug. 2008.

[14] Heniche, A., Kamwa, I., "Assessment of two methods to select wide-area signals for power system damping control," *IEEE Trans. on Power Syst.*, vol. 23, no. 2, pp. 572-581, May 2008.

[15] A. Heniche and I. Kamwa, "Control loops selection to damp inter-area oscillations of electric networks," *IEEE Trans. on Power Syst.*, vol. 17, no. 2, pp. 378-384, May 2002.

[16] A. Vaccaro and D. Villacci, "Radial power flow tolerance analysis by interval constraint propagation," *IEEE Trans on Power Syst.*, vol. 24, no.1, pp. 28-39, Jan. 2009.

[17] V. Puig, J. Quevedo, T. Escobet, F. Nejjari, and S. de las Heras, "Passive robust fault detection of dynamic processes using interval models", *IEEE Trans. on Contr. Syst. Tech.*, vol. 16, no. 5, pp. 1083-1089, Sept. 2008.

[18] A. C. Bartlett, C. V. Hollot, and L. Huang, "Root locations of an entire polytope of polynomials: It Suffices to check the edges" in *Amer. Contr. Conf.*, pp. 1611 – 1616, Jun. 1987.

[19] B. R. Barmish, M. Fu, and S. Saleh, "Stability of a polytope of matrices: counter examples", *IEEE Trans. Automat. Contr.*, vol. 33, no. 6, pp. 569-752, Jun. 1988.

[20] B. R. Barmish, "A generalization of Karitonov's four polynomial concept for robust stability problems with dependent coefficient perturbations", *IEEE Trans. Automat. Contr.*, vol. 34, no. 2, pp. 157-165, Feb. 1989.

[21] S.-H. Chen, H.-D. Lian. X.-W. Yang, "Interval eigenvalue analysis for structures with interval parameters", *Finite Elements in Analysis and Design*, vol. 39, issues 5-6, pp. 419-431, Mar. 2003.

[22] S. Adhikari and M. I. Friswell, "Random matrix eigenvalue problems in structural dynamics", *International Journal of Numerical Methods in Engineering*, vol. 69, no. 3, pp. 562-591, 2007.

[23] X.-M. Zhang, Y.-D. Chen, S.-H. Chen, and C.-Y. Pei, "Interval eigenvalues of closed-loop systems of uncertain structures," *ACTA Mechanica Solida Sinica*, vol. 26, no. 2, pp. 182-186, Jun. 2005.

[24] Dotta, D.; e Silva, A.S.; Decker, I.C., "Wide-area measurements-based two-level control design considering signal transmission delay," *IEEE Trans on Power Syst.*, vol. 24, no.1, pp. 208-216, Feb. 2009.